QUARTERLY JOURNAL OF THE ROYAL METEOROLOGICAL SOCIETY
Q. J. R. Meteorol. Soc. **135**: 1950–1967 (2009)
Published online 3 August 2009 in Wiley InterScience
(www.interscience.wiley.com) DOI: 10.1002/qj.455

An overview of barrier winds off southeastern Greenland during the Greenland Flow Distortion experiment

G. N. Petersen,[a]* I. A. Renfrew[a] and G. W. K. Moore[b]
[a]*School of Environmental Sciences, University of East Anglia, UK*
[b]*Department of Physics, University of Toronto, Canada*

ABSTRACT: During the Greenland Flow Distortion experiment, barrier flow was observed by an instrumented aircraft on 1, 2, 5 and 6 March 2007 off southeastern Greenland. During this time period the barrier flow increased from a narrow jet, $\sim 15\,\mathrm{m\,s^{-1}}$, to a jet filling almost the whole of the Denmark Strait with maximum wind speed exceeding $40\,\mathrm{m\,s^{-1}}$. Dropsonde observations show that the barrier flow was capped by a sharp temperature inversion below mountain height. Below the inversion was a cold and dry jet, with a larger northerly wind component than that of the flow above, which was also warmer and more moist. Thus, the observations indicate two air masses below mountain height: a cold and dry barrier jet of northern origin and, above this, a warmer and moister air mass that was of cyclonic origin.

Numerical simulations emphasize the non-stationarity of the Greenland barrier flow and its dependence on the synoptic situation in the Greenland–Iceland region. They show that the barrier jet originated north of the Denmark Strait and was drawn southward by a synoptic-scale cyclone, with the strength and location of the maximum winds highly dependent on the location of the cyclone relative to the orography of Greenland. Experiments without Greenland's orography suggest a $\sim 20\,\mathrm{m\,s^{-1}}$ enhancement of the low-level peak wind speeds due to the presence of the barrier. Thus, the Greenland barrier flows are not classic geostrophically balanced barrier flows but have a significant ageostrophic component and are precisely controlled by synoptic-scale systems. Copyright © 2009 Royal Meteorological Society

KEY WORDS Greenland Flow Distortion experiment; Barrier flow; FAAM; observations; orographic flow; MetUM

Received 5 December 2008; Revised 24 April 2009; Accepted 13 May 2009

1. Introduction

Atmospheric flow is significantly influenced by mountains; the mid-tropospheric troughs formed by the Rocky Mountains and the Tibetan Plateau are excellent examples of the global impact of major mountain ridges. On a smaller scale, mountains can induce significant wind phenomena such as föhn winds, downslope wind storms, katabatic winds and barrier winds, often resulting in high-impact weather (e.g. von Hann, 1866; Durran, 1990; Heinemann, 1999).

Barrier winds typically occur when cold and stably stratified air is forced by synoptic-scale flow towards a topographic barrier. If the non-dimensional mountain height, $\hat{h} = Nh/U$, where N is the Brunt–Väisälä frequency, h the mountain height and U the upstream wind component normal to the barrier, is sufficiently large then the air is unable to cross the barrier. Instead, the flow is blocked and there is a damming of the air against the barrier. A pressure gradient develops perpendicular to the barrier, resulting in an approximately geostrophic flow along the barrier (Schwerdtfeger, 1975; Parish, 1983). Barrier flow can be found along many mountain ranges, for example the Antarctic Peninsula (Schwerdtfeger, 1975), the Rocky Mountains (Colle and Mass, 1995), the Appalachians (Bell and Bosart, 1988), the Sierra Nevada (Parish, 1982) and the Alps (Chen and Smith, 1987). Barrier winds are often associated with a cold-air surge (e.g. Schwerdtfeger, 1975; Bell and Bosart, 1988) but have also been found to enhance pre-frontal rainfall (Revell *et al.*, 2002). Perhaps the most classical barrier flow is found along the Antarctic Peninsula. In other locations the barrier flow is often more complicated due to the synoptic situation or complexity of the orography. For example, Loescher *et al.* (2006) investigated the barrier flow along the Alaskan coast and identified two types: a classic barrier flow where the low-level jet is primarily fed by onshore air and a hybrid barrier flow where the low-level jet is primarily fed by gap flow from the continental interior. Another example is the Appalachian barrier flow, which originates far north of the mountains but becomes a barrier flow as it reaches the Appalachians, where it is controlled by the synoptic situation (Bell and Bosart, 1988).

The oceans surrounding Greenland are known for extreme weather in the wintertime. West of Greenland, over the Labrador Sea, there are frequently cold-air outbreaks and developments of intense mesoscale cyclones (Renfrew and Moore, 1999; Pagowski and Moore, 2001). There have been observations of barrier winds at the western margin of the Greenland ice sheet. These winds

*Correspondence to: G. N. Petersen, School of Environmental Sciences, University of East Anglia, Norwich, NR4 7TJ, UK.
E-mail: gnp@vedur.is

were identified as thermally forced jets, enhanced by the topography (van den Broeke and Gallée, 1996). East of Greenland, the Greenland–Iceland region is recognized for its frequent cyclone activity, with a climatological cyclone over Iceland in the wintertime. The high orography of Greenland has a large impact on the atmospheric flow in the North Atlantic region (Scorer, 1988; Petersen *et al.*, 2003). Frequently, quasi-barotropic cyclones form behind baroclinic cyclones in the Greenland–Iceland region and there is evidence that the orography of Greenland is important for this development (Kristjánsson and McInnes, 1999; Skeie *et al.*, 2006). The orography also modifies the ambient airflow in the region, resulting in strong low-level winds close to the coast that are a potential maritime hazard. It has even been suggested that this orographic enhancement is the reason that the region of Cape Farewell, the southern tip of Greenland, is the windiest location on the ocean's surface (Sampe and Xie, 2007). Doyle and Shapiro (1999) investigated the dynamics of low-level westerly wind jets, termed tip jets, emanating from Cape Farewell. They found the orographic deflection of the airflow around the cape and Lagrangian acceleration on the slope to be the deciding factors in the strength of the tip jet. Moore and Renfrew (2005) compiled a climatology of high-wind-speed events around southern Greenland using a QuikSCAT data set. In addition to westerly tip jets, they also found easterly high-wind-speed events at Cape Farewell, the so-called reverse, or easterly, tip jets first described by Moore (2003). Farther north along the southeastern coast of Greenland, they identified two regions with frequent barrier flow, which they termed Denmark Strait South and Denmark Strait North.[†]

These barrier winds are interesting local meteorological phenomena, but they may also be of importance on larger spatial and temporal scales. It has been proposed, for example, that the strong winds in the region may play a major role in the global ocean circulation, as the associated high air–sea heat fluxes lead to densification of the surface ocean, water-mass changes and possibly ocean overturning (e.g. Pickart *et al.*, 2003a,b; Haine *et al.*, 2009). The barrier flow may therefore play a role in the global ocean circulation.

As this is a sparsely populated region with extreme weather conditions, there are few meteorological stations and, due to sea ice, no surface winds can be derived from satellite data close to the coast of Greenland. Furthermore, satellite-derived winds, being surface winds, contain no information about the vertical structure of the wind field. It was therefore clear that in order to acquire insight into the mesoscale flow in the region a field campaign was necessary. Indeed, one of the main goals of the Greenland Flow Distortion experiment (GFDex) was to obtain *in situ* observations of mesoscale weather phenomena in the Greenland–Iceland region. In the current article we present an overview of the barrier flow off southeastern Greenland during the GFDex. The region of interest is shown in Figure 1. We present unique dropsonde observations of the barrier flow. The observations are placed in synoptic context and discussed with the support of meteorological analyses and high-resolution numerical simulations. We believe these represent the first comprehensive observations of barrier flow off southeast Greenland and the first aircraft-based observations.

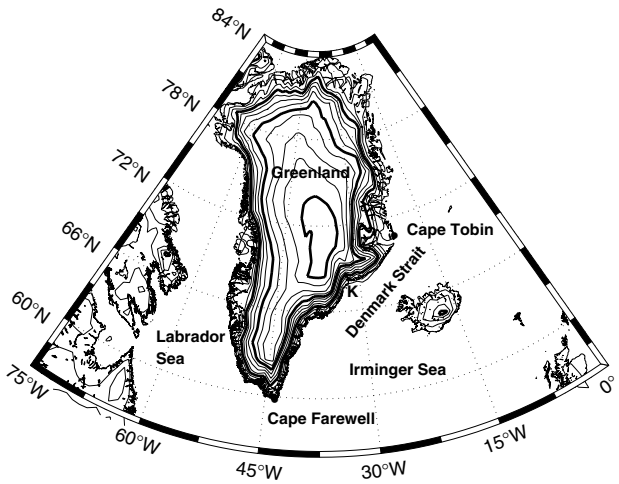

Figure 1. A map showing the topography (m) in the region of interest. The height contours are shown every 250 m and every 1000 m contour is shown in bold. Kangerdlussuaq fjord is marked with the letter K.

The article has the following structure. The next section introduces GFDex and the barrier flow missions discussed in the article. Dropsonde observations are described in section 3 and results from numerical simulations are presented in section 4. Section 5 provides a discussion of the findings and finally some concluding remarks are made in section 6.

2. The Greenland Flow Distortion experiment

GFDex is an international project investigating the role of Greenland in defining the structure and predictability of both local and downstream weather systems. The field campaign, which took place for three weeks in February and March 2007, was primarily aircraft-based, utilizing the specially instrumented Facility for Airborne Atmospheric Measurements (FAAM) BAE-146 aircraft, but there were also additional radiosonde releases in the region during the campaign. An overview of the experiment, the objectives, logistics and missions can be found in Renfrew *et al.* (2008).

Of the 12 missions that were flown, barrier flow was observed in four missions, on 1, 2, 5 and 6 March. On 1 March a weak barrier flow was driven by two mesoscale cyclones; while on the other days the barrier flow was stronger and driven by synoptic-scale cyclones. Most of the barrier flow observations were made using GPS dropsondes that measured a vertical profile of the atmosphere. In two missions aircraft observations at lower levels were also made. However, here we

[†]Note that Moore and Renfrew's Denmark Strait South location is at the southern edge of the Denmark Strait, while their Denmark Strait North composite shows strong winds in most of the Denmark Strait (their Figures 12 and 13).

DOI: 10.1002/qj

Table I. A summary of dropsonde flight legs, time of day and number of sondes.

Mission	Date	Time of day UTC	Flight leg	No. of dropsondes
B273	1 March	1152–1231	Denmark Strait South (DSS)	4
B273	1 March	1252–1325	Denmark Strait North (DSN)	5
B274	2 March	1136–1210	Denmark Strait South (DSS)	5
B274	2 March	1231–1303	Denmark Strait North (DSN)	4
B277	6 March	1409–1436	North of Denmark Strait (NoDS)	8
B277	6 March	1444–1526	Denmark Strait North (DSN)	8

concentrate on the dropsonde observations in and north of the Denmark Strait, as they provide a concise overview of the vertical and horizontal structure of the flow.

The GPS dropsondes (Vaisala RD93) measure the position, altitude, pressure, temperature and relative humidity at 2 Hz and calculate the wind speed and wind direction. For dropsondes terminating at the sea surface the GPS-determined altitude is corrected from the ground upwards. For dropsondes terminating over land the altitude is instead computed by downward integration from a launch altitude provided by the aircraft data system. The quality-control procedures involved outlier checks (using 10 standard deviations for each variable), filtering of suspect data points, pressure smoothing, temperature dynamic adjustment and wind dynamic adjustment. Buddy checks were applied for pressure, temperature, relative humidity and the winds using thresholds per second of 2 hPa, 3°C, 20% and 5 m s^{-1} respectively. A 10 second filter was also applied to the same variables, with deviation limits of 3 hPa, 3°C, 3% and 3 m s^{-1}. There is a final smoothing over a 5 s period (10 s for winds). Note that these dropsondes typically fall at about 10 m s^{-1}. The accuracy (repeatability) of the soundings is 0.4 hPa, 0.1°C, 2% and 0.5 m s^{-1} for pressure, temperature, relative humidity and winds, respectively. Further details on the quality-control procedures can be found in the ASPEN User Manual (Martin, 2007).

Sondes were dropped along three flight legs (see Figure 2): along two flight legs in the Denmark Strait, termed 'Denmark Strait South' (DSS) and 'Denmark Strait North' (DSN) as well as along 69°50′N, here termed 'North of Denmark Strait' (NoDS). Table I lists the dates, times and the number of sondes launched for each dropsonde leg. Although in some cases the sondes were dropped 2–3 hours after noon, for most purposes it is reasonable to consider analysis and numerical simulations at 1200 UTC. (Note that at 1200 UTC the time in Iceland is 1200 local time while in Greenland the time is 0900 local time. Thus, to avoid any confusion all times are given in UTC.) Note that one other dropsonde leg was carried out on 5 March 2009, but much further south, about 65°N, 32°W, and so will not be discussed in this article.

Figure 2 shows the mean sea level pressure analyses and the 500 hPa height from the European Centre for Medium-Range Weather Forecasts (ECMWF) at 1200 UTC on 1–6 March 2007. On 1 March (Figure 2(a)), a 986 hPa barotropic synoptic cyclone was located about 900 km east-southeast of Cape Farewell. Just west of Iceland there was a 990 hPa mesoscale cyclone and east of northern Greenland a 972 hPa long-lived mesoscale cyclone, discussed briefly in Renfrew *et al.* (2008). The air flow at lower levels in the Denmark Strait was dominated by the influence of these two mesoscale cyclones. At the 500 hPa level a low was located over the northeastern coast of Greenland. There was therefore a decoupling between the low- and mid-tropospheric flow in the Denmark Strait, with northeasterly flow at lower levels and westerly flow at higher levels.

During the next few days, the synoptic cyclone moved northward over the Irminger Sea, deepening by 8 hPa in the first 24 hours (see Figure 2(b)). It dominated the situation for the next few days, circulating in the Greenland–Iceland region. At mid-tropospheric levels a trough developed over Greenland on 2 March (see Figure 2(b)). It moved to the east and connected to the surface cyclone on 3 March, moving the centre close to the orography and deepening the cyclone slightly (Figure 2(c)). Observations were obtained in the cyclone centre on 3 March and are presented in McInnes *et al.* (2009). On 4 March another barotropic cyclone, stationed south of Iceland (at 55°N, 15°W) at 1200 UTC (Figure 2(d)), moved into the region. It was incorporated into the main low and decreased the lowest pressure in the region by about 20 hPa in the 24 h prior to 1200 UTC on 5 March, when the centre pressure was 955 hPa (Figure 2(e)). On 5 and 6 March there was a cyclonic circulation in the whole Greenland–Iceland region at both low- and mid-tropospheric levels and thus no longer a decoupling with height of the flow in the Denmark Strait.

3. Dropsonde observations of the barrier flows

The ECMWF analysis on 2 March (Figure 2(b)) resembles, in many ways, the barrier flow in the Denmark Strait South composite of Moore and Renfrew (2005) (their Figure 12) with a synoptic cyclone over the Irminger Sea dominating the atmospheric flow in the Greenland–Iceland region. Similarly, the analysis on 5–6 March (Figure 2(e)–(f)) has similarities with Moore and Renfrew (2005) barrier flow in the Denmark Strait North composite. Although the synoptic situation on 2–6 March is mainly dominated by the same synoptic cyclone, it seems natural to divide the presentation of the observations into these two barrier flow phases.

DOI: 10.1002/qj

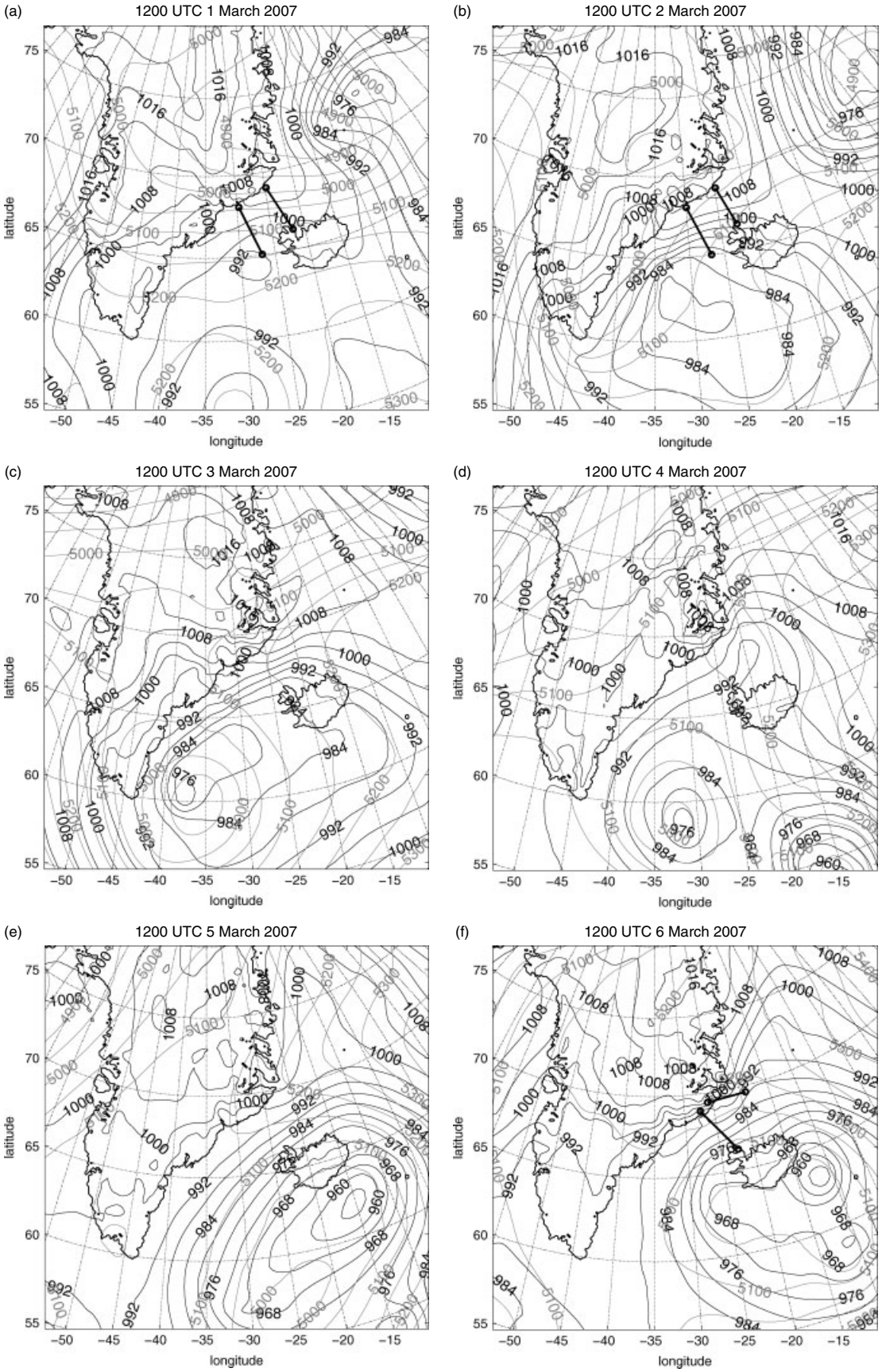

Figure 2. ECMWF analysis of mean sea level pressure (hPa, black) and 500 hPa geopotential height (m, grey) at 1200 UTC on (a) 1 March, (b) 2 March, (c) 3 March, (d) 4 March, (e) 5 March and (f) 6 March 2007. The locations of dropsonde flight legs are marked in bold: in (a) and (b) DSS (Denmark Strait South) and DSN (Denmark Strait North) flight legs and in (f) DSN (Denmark Strait North) and NoDS (North of the Denmark Strait). The contour interval is 4 hPa for pressure and 50 m for geopotential height.

DOI: 10.1002/qj

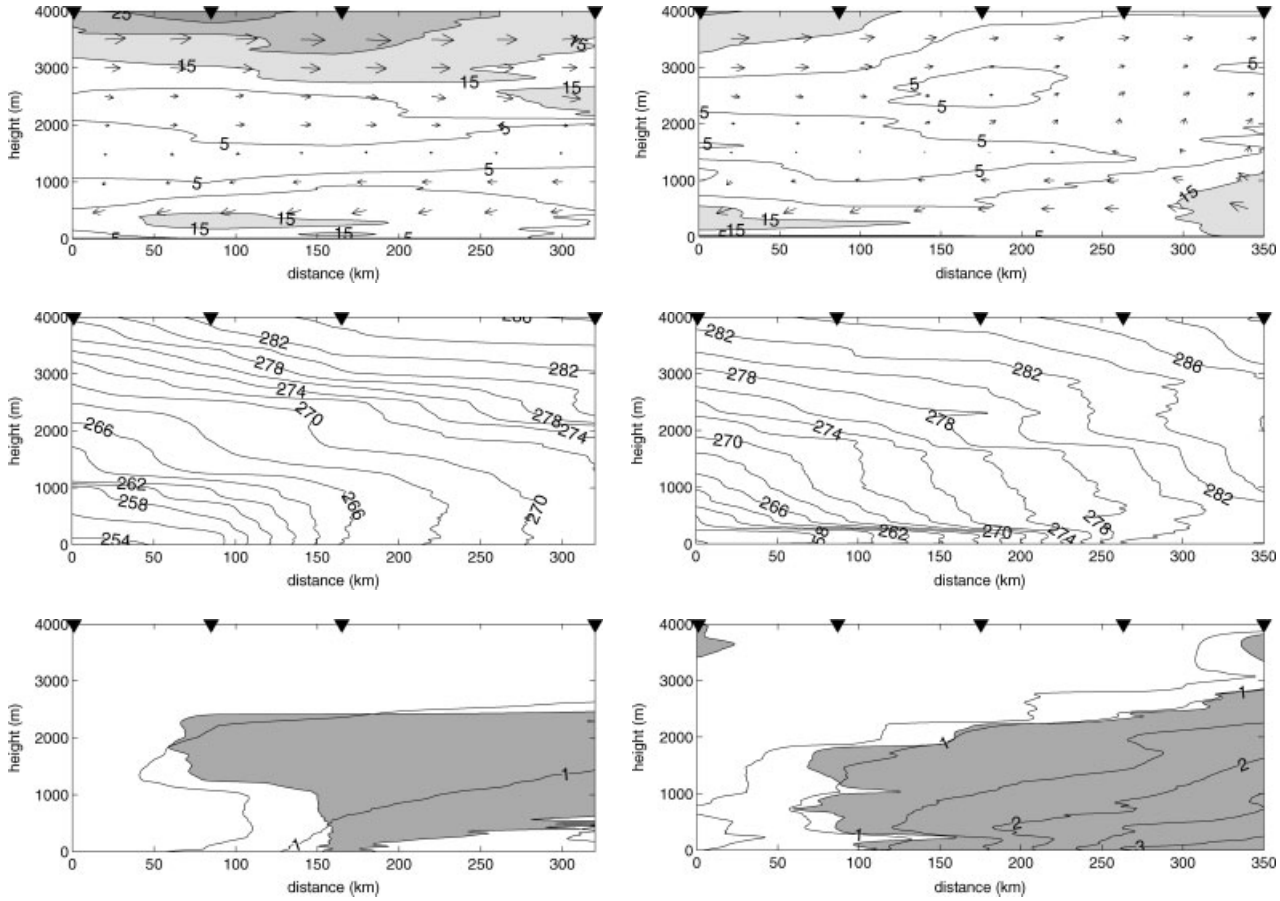

Figure 3. 1 March 2007: horizontally interpolated dropsonde observations. Left panels show the DSN cross-section and right panels the DSS cross-section. Top: wind speed ($m\,s^{-1}$) and horizontal wind vectors showing the wind direction. The contour interval is $5\,m\,s^{-1}$ and wind speeds exceeding $15\,m\,s^{-1}$ are shaded. Centre: equivalent potential temperature (K), contour interval 2 K. Bottom: specific humidity ($g\,kg^{-1}$), contour interval $0.5\,g\,kg^{-1}$ with shading of relative humidity exceeding 80%. The distance axis is southeastward, away from the Greenland coast. The triangles show the location of the dropsondes along the flight leg.

3.1. Barrier flow observations: 1–2 March 2007

On 1 and 2 March dropsondes were launched along flight legs DSN and DSS (Figure 2(a)–(b)). The synoptic situation changed dramatically between these two consecutive days, with a mesoscale cyclone forcing a weak pressure gradient in the Denmark Strait region on 1 March, in contrast to a synoptic cyclone forcing a strong pressure gradient 24 hours later. On 2 March the largest pressure gradient was found south of the Denmark Strait (see Figure 2(b)), and thus the observations were made upstream of the strongest low-level flow. To generate cross-sections, the dropsonde soundings were linearly interpolated onto a regular height grid of resolution 10 m, then linearly interpolated onto a regular distance grid of 10 km. Figure 3 shows interpolated cross-sections from the dropsondes released along the flight legs on 1 March (see Figure 2(a)), with the locations of the dropsondes marked with a triangle at the top. In the northern cross-section (DSN: top left panel) there was a shallow east–northeasterly low-level jet in the middle of the Denmark Strait. Farther south, in the southern cross-section (DSS: top right panel), the jet had moved closer to the coast of Greenland. Above the jet, extending up to the mountain height (roughly 3000 m), there was a calm layer, with wind speeds $\leq 10\,m\,s^{-1}$, before the wind speed increased again in the upper-level westerly jet. The easternmost dropsonde of the southern leg descended into the mesoscale cyclone just west of Iceland (see Figure 2(a)). Here, the observed wind speeds were comparable to the barrier winds ($15–19\,m\,s^{-1}$), but the winds associated with the mesoscale cyclone extended farther vertically, up to about 1500 m, and had a southerly component (Figure 3, top right panel).

The centre panels show equivalent potential temperature cross-sections. The sea ice extended from Greenland for about 150 km and 220 km along the northern and southern cross-sections, respectively. Over open water the surface layer was conditionally unstable, while the atmospheric boundary layer (ABL) was approximately neutrally stratified. On the other hand, over the sea ice the atmosphere was stably stratified from the surface upwards, with a strong temperature inversion at about 200 m above the sea ice along the southern cross-section. Over the open water, and to some extent over the sea ice, a distinct temperature inversion can be detected at about 1800 m, indicating the top of the ABL.

Over the sea ice, close to the coast of Greenland, the air was dry, while the well-mixed boundary layer over the open ocean was moist with specific humidity exceeding

DOI: 10.1002/qj

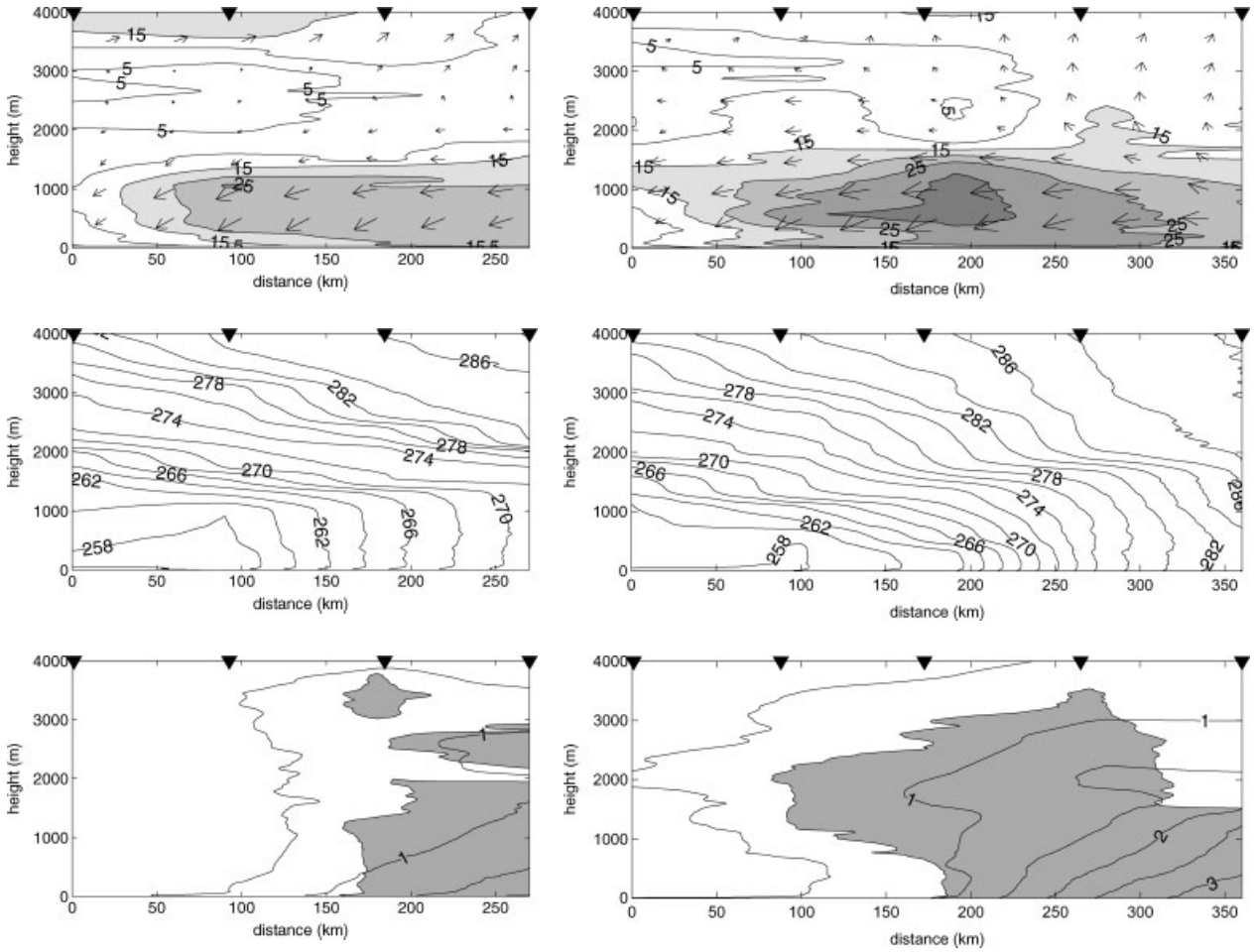

Figure 4. 2 March 2007: horizontally interpolated dropsonde observations. Left panels show the DSN cross-section and right panels the DSS cross-section. Top: wind speed ($m\,s^{-1}$) and horizontal wind vectors indicating wind direction. The contour interval is $5\,m\,s^{-1}$ and wind speeds exceeding $15\,m\,s^{-1}$ are shaded. Centre: equivalent potential temperature (K), contour interval 2 K. Bottom: specific humidity ($g\,kg^{-1}$), contour interval $0.5\,g\,kg^{-1}$ with shading of relative humidity exceeding 80%. The distance axis is southeastward, away from the Greenland coast. The triangles show the location of the dropsondes along the flight leg.

$2\,g\,kg^{-1}$ at the southeastern edge of the southern cross-section (right-hand side). Note the moist air above the sea-ice edge, especially in the southern cross-section, providing evidence that the mixed layer above the low-level inversion was advected from open water.

During the next 24 hours the synoptic cyclone moved northward, over the Irminger Sea, and started dominating the situation. This resulted in a much larger pressure gradient along the southeast coast of Greenland (see Figure 2(b)), and thus much stronger barrier flow on 2 March than the previous day. Figure 4 shows the interpolated cross-sections for the DSN and DSS dropsonde legs on 2 March (see Figure 2(b)). Note that the extent of the cross-sections is slightly different than in Figure 3, as the exact locations of the dropsondes may vary. The differences in the winds compared with the day before are clear. The east–northeasterly barrier flow almost fills the whole of the Denmark Strait below 1800 m. The maximum wind speed was $25\,m\,s^{-1}$ in the northern cross-section (top left panel) and $31\,m\,s^{-1}$ in the southern cross-section (top right panel), in both cases close to the centre of the Denmark Strait. Note that at the lowest levels there were lower wind speeds over the sea ice, on the northwest side of the cross-section (left-hand side), than over the open water. This may be related to a larger surface roughness in the presence of sea ice. In other ways the situation was similar to the one on the previous day: again there was a calm layer above the jet and increasing southwesterly winds above the mountain height.

Over the sea ice a stable ABL layer can be detected. Over the open ocean there was a shallow surface layer, absolutely unstable along the northern cross-section but conditionally unstable along the southern cross-section. Above the surface layer the ABL was well mixed and approximately neutrally stratified, capped by a strong temperature inversion at about 1500–1800 m height. Note that the air above the inversion in the southeastern part of the DSS cross-section (right-hand side) was less stable than elsewhere above the inversion, and here the winds were stronger and had a southerly wind direction. As expected, the air is dry over the sea ice but relatively moist over the open water. Furthermore, at the southeastern side of the cross-sections (right-hand side) the specific humidity of the air just above the temperature inversion was higher than for the air just below, indicating

DOI: 10.1002/qj

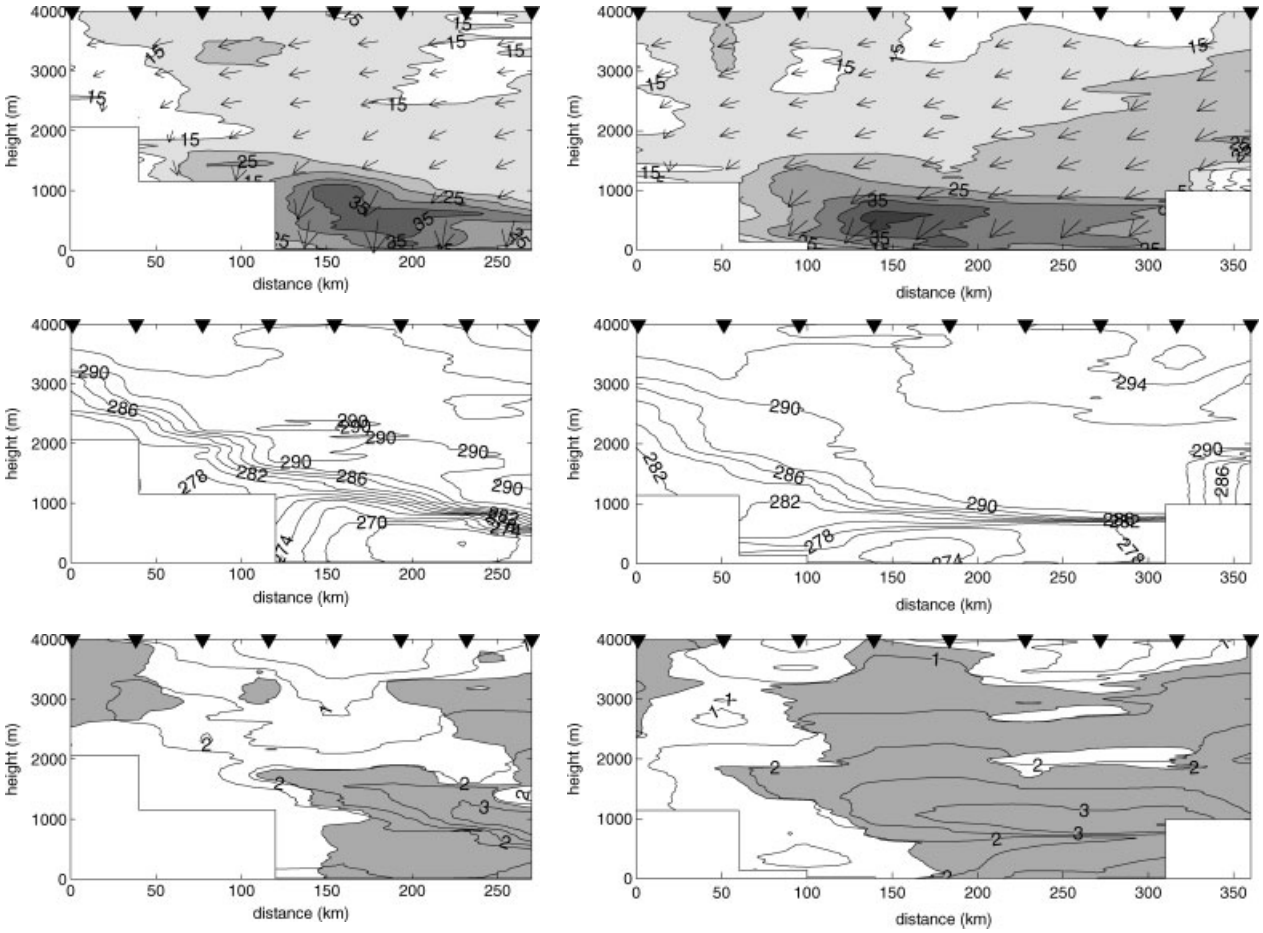

Figure 5. 6 March 2007: horizontally interpolated dropsonde observations. Left panels show the NoDS cross-section and right panels the DSN cross-section. Top: wind speed ($m\,s^{-1}$) and horizontal wind vectors indicating wind direction. The contour interval is $5\,m\,s^{-1}$ and wind speeds exceeding $15\,m\,s^{-1}$ are shaded. Centre: equivalent potential temperature (K), contour interval 2 K. Bottom: specific humidity ($g\,kg^{-1}$), contour interval $0.5\,g\,kg^{-1}$ with shading of relative humidity exceeding 80%. The distance axis is eastward in the left column and southeastward in the right column, away from the Greenland coast. The triangles show the location of the dropsondes along the flight leg and the white boxes represent areas with no data, e.g. where the dropsondes landed on elevated land.

that there may be two separate air masses below and above the temperature inversion.

The observations on these two consecutive days show a dramatic change in the barrier flow, with a weak and narrow $15\,m\,s^{-1}$ jet on 1 March but a strong and broad $31\,m\,s^{-1}$ jet on 2 March, filling almost the whole strait. However, there are also similarities, such as the ABL height being similar, capped by a temperature inversion at about 1500–1800 m, and a drop in wind speed and changed wind direction above the inversion.

3.2. Barrier flow observations: 6 March 2007

On 6 March dropsondes were launched both north of the Denmark Strait, along 69°50′N (NoDS) and along the DSN flight leg. At that time the cyclone centre was located by the southeast coast of Iceland and the pressure gradient in the Denmark Strait was large (see Figure 2(f)). The barrier flow was very strong, the maximum wind speed exceeding $35\,m\,s^{-1}$ north of the Denmark Strait and $40\,m\,s^{-1}$ in the Denmark Strait (Figure 5). In the NoDS cross-section (top left panel) the maximum wind speed was found close the the coast, but in the DSN cross-section (top right panel) the maximum was farther away from the coast. Note the lower wind speeds in the lowest levels on the western side (LHS) of the cross-sections compared with the eastern side – again this is most likely due to the the larger surface roughness in the presence of sea ice than over open water. The barrier flow covered most of the DSN cross-section below about 1000 m. However, above there were still strong winds, 15–$25\,m\,s^{-1}$, and little change in wind direction with height.

The equivalent potential temperature cross-sections (centre panels) show that the boundary layer was mainly neutral in stratification, with a very cold core. In the DSN cross-section (right panel), close to the coast of Greenland over ice-covered ocean, there was a stable ABL. At the top of the low-level jet there was an extremely strong temperature inversion that increased its height over land in the NoDS cross-section. Above this inversion the air was slightly stable or neutrally stratified.

There was a clear difference in the humidity of the air above and below the temperature inversion: while the air above the inversion was moist, with the specific humidity exceeding $3\,g\,kg^{-1}$ just above the inversion, the

DOI: 10.1002/qj

air below was very dry (<1.5 g kg^{-1}; see Figure 5, bottom panels).

In summary, there are several features that distinguish the air in the low-level jet from the air above. The wind direction was slightly more northerly in the jet than in the air above, the jet had a very cold and dry core and was confined below a strong temperature inversion. All this indicates that two air masses with different origin were observed below mountain height, and this is investigated further in the next section.

4. Numerical simulations

4.1. Model set-up

The barrier flow cases were simulated using the atmosphere-only mode of the UK Met Office Unified Model (MetUM), ported version 6.1. The Unified Model is a non-hydrostatic model with a semi-implicit, semi-Lagrangian numerical scheme (Davies *et al.*, 2005) and a comprehensive set of parametrizations, e.g. in the boundary layer (Lock *et al.*, 2000; Martin *et al.*, 2000) and at the surface (Essery *et al.*, 2001). The subgrid-scale orographic scheme is a flow-blocking and gravity-wave drag scheme (Webster *et al.*, 2003). In limited-area mode the model is run on a rotated latitude–longitude horizontal grid with Arakawa C staggering and a terrain-following hybrid-height vertical coordinate with Charney–Philips staggering. The barrier-flow cases were run with a horizontal grid length of 0.11° (approximately 12 km) and 220×220 grid points in the horizontal. This is the same domain as shown in Figure 2. In the vertical there are 76 non-uniformly spaced levels, of which 26 levels are in the boundary layer.

The initial and boundary conditions were provided by the UK Met Office operational global MetUM forecasts. The only exceptions are the sea-ice concentration and sea-surface temperature (SST) fields, where data from the Operational Sea Surface Temperature and Sea Ice Analysis (OSTIA) were used. The OSTIA data set has been developed by the UK Met Office (http://ghrsst-pp.metoffice.com/pages/latest_analysis/ostia.html). The output is a daily, global coverage 1/20° (~ 6 km) combined SST and sea-ice concentration product, which is generated in near-real time. The analysis is designed to provide accurate SSTs suitable for numerical weather prediction at global and regional space- and time-scales (Stark *et al.*, 2007). The SST fields have been used operationally by the UK Met Office in the global forecast suite since 2 October 2007 and in the North Atlantic–Europe limited-area suite since 27 November 2007. The sea-ice analysis was implemented operationally in both suites on 22 July 2007 (Rachel North, personal communication). The OSTIA data set captures mesoscale features such as SST fronts much better than the default SST. This is especially important in the Greenland–Iceland region, due to large SST gradients and the vicinity of the sea-ice edge (Outten *et al.*, 2009). However, although the OSTIA SST data set has been shown to be superior to the earlier SST analysis used at the UK Met Office (Stark *et al.*, 2007), comparison to GFDex aircraft observations suggests a slight warm bias in the Greenland–Iceland region (Petersen and Renfrew, 2009; Renfrew *et al.*, 2009).

In the parametrization of air–sea turbulent fluxes, the MetUM uses a linear combination of three surface roughness lengths where sea ice is present: $Z_{0\,ice}$, $Z_{0\,MIZ}$ and $Z_{0\,sea}$, representing values over ice-covered ocean, in the marginal ice zone (MIZ) and over open water, respectively. In a comparison of simulations using the default values, $Z_{0\,ice} = 3.0 \times 10^{-3}$ m and $Z_{0\,MIZ} = 1.0 \times 10^{-1}$ m, against the GFDex observations these values were found to be too high, resulting in a local minimum in wind speed at the ice edge that was not observed. The values were therefore decreased to $Z_{0\,ice} = Z_{0\,MIZ} = 5.0 \times 10^{-4}$ m, the same values as used in the Met Office Hadley Centre MetUM climate configuration (Edwards, 2007). These values are in better agreement with observations than the default values (e.g. Andreas *et al.*, 2005; Lüpkes and Birnbaum, 2005; Brunke *et al.*, 2006).

The barrier flows were simulated with two simulations: the first was initialized at 0000 UTC on 1 March and ran for 48 hours; the second was initialized at 0000 UTC on 5 March and ran for 48 hours. Therefore the first simulation covers the cases with maximum barrier wind south of the Denmark Strait (Figures 3 and 4) while the second simulation covers the strong barrier flow in the Denmark Strait (Figure 5).

4.2. Simulated barrier flow: 1–2 March 2007

Figures 6 and 7 show the simulated mean sea level pressure and barrier flow evolution at 650 m height, roughly the height of maximum wind speed, from 1200 UTC 1 March to 1200 UTC 2 March, every 12 hours. The simulation does not capture the mesoscale cyclone just west of Iceland properly at 1200 UTC on 1 March (compare Figure 6(a) with Figure 2(a)), but otherwise the pressure field is in good agreement with the analysis. During the simulation, as the mesoscale cyclone to the north of Iceland moves eastward and the synoptic cyclone moves northward over the Irminger Sea, the pressure gradient perpendicular to the southeast coast of Greenland increases (Figure 6(c)). During the whole simulation the air flows southward along the northeastern coast of Greenland, forced by the mesoscale cyclone north of Iceland (Figure 7(a)). South of Cape Tobin the flow splits with part of it flowing around the mesoscale cyclone (east of Iceland) while the rest of the air flows *across* the isobars through the Denmark Strait and then onwards along the southeastern coast of Greenland. Thus, there appears to be a significant ageostrophic component to the flow in the Denmark Strait. The simulated flow in the DSS cross-section at 1200 UTC on 1 March is shown in Figure 8. The low-level jet is not as narrow as observed (in Figure 3, top right panel) and extends farther into the Denmark Strait, but as observed the jet is capped by a calm layer. The equivalent potential temperature cross-section is in relatively good agreement

DOI: 10.1002/qj

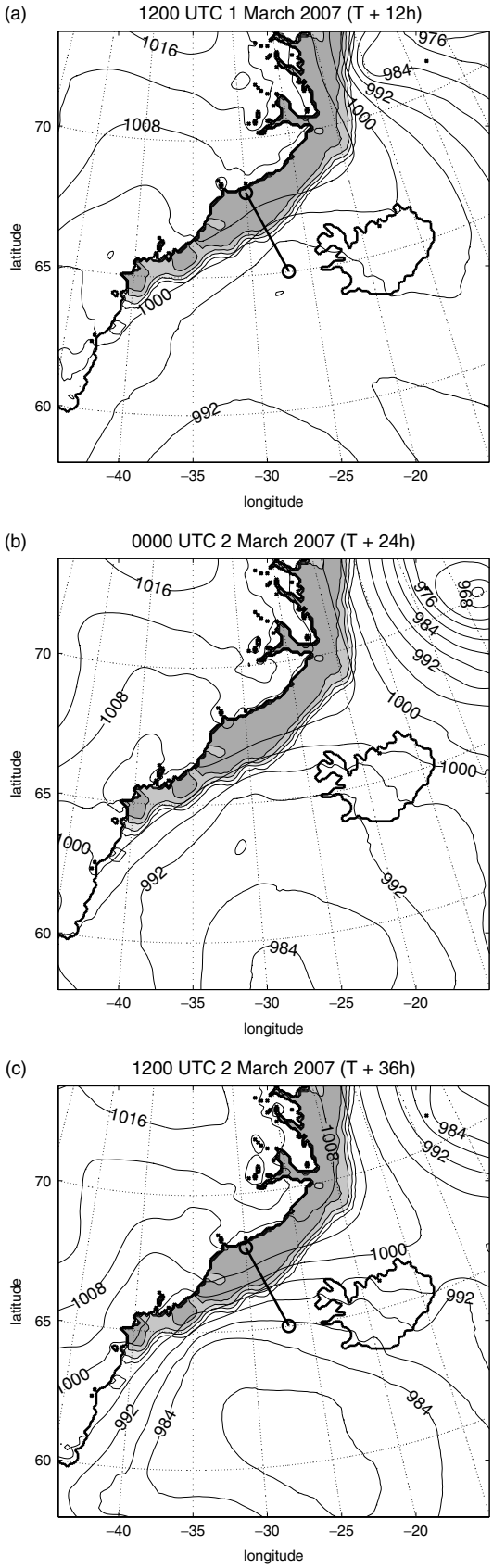

Figure 6. Simulated barrier flow for 1–2 March 2007: mean sea level pressure (hPa). The simulation is initialized at 0000 UTC on 1 March. (a) 1200 UTC 1 March (T + 12 h), (b) 0000 UTC 2 March (T + 24 h) and (c) 1200 UTC 2 March (T + 36 h). The contour interval is 4 hPa. The shaded area represents the sea-ice concentration, shading interval 0.2. The bold lines represent the DSS cross-section.

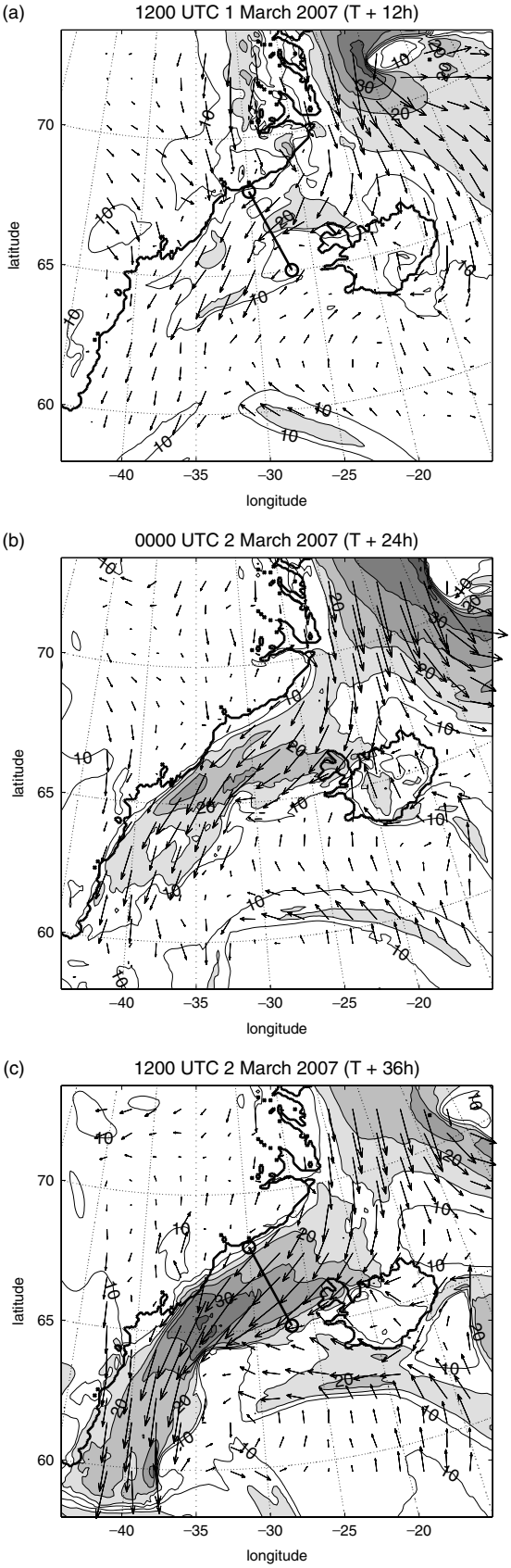

Figure 7. Simulated barrier flow for 1–2 March: wind speed ($m\,s^{-1}$, solid) and wind vectors at model level 12 ($\sim$ 650 m). The simulation is initialized at 0000 UTC on 1 March. (a) 1200 UTC 1 March (T + 12 h), (b) 0000 UTC 2 March (T + 24 h) and (c) 1200 UTC 2 March (T + 36 h). The contour interval is 5 $m\,s^{-1}$ and wind speeds exceeding 15 $m\,s^{-1}$ are shaded. The bold line represents the DSS cross-section.

DOI: 10.1002/qj

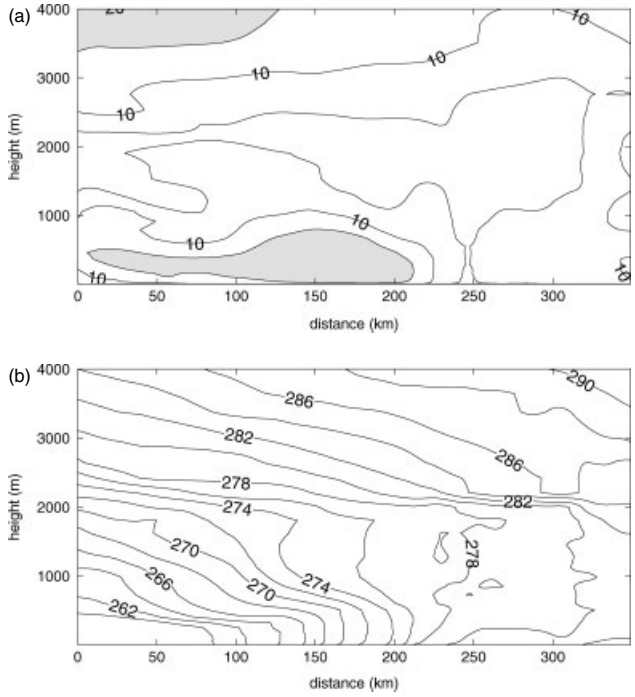

Figure 8. Simulated barrier flow at 1200 UTC on 1 March (T + 12 h) in the DSS cross-section, see Figure 6(a) for location. (a) Wind speed ($m\,s^{-1}$), contour interval 5 $m\,s^{-1}$ with wind speeds exceeding 15 $m\,s^{-1}$ shaded. (b) Equivalent potential temperature (K), contour interval 2 K.

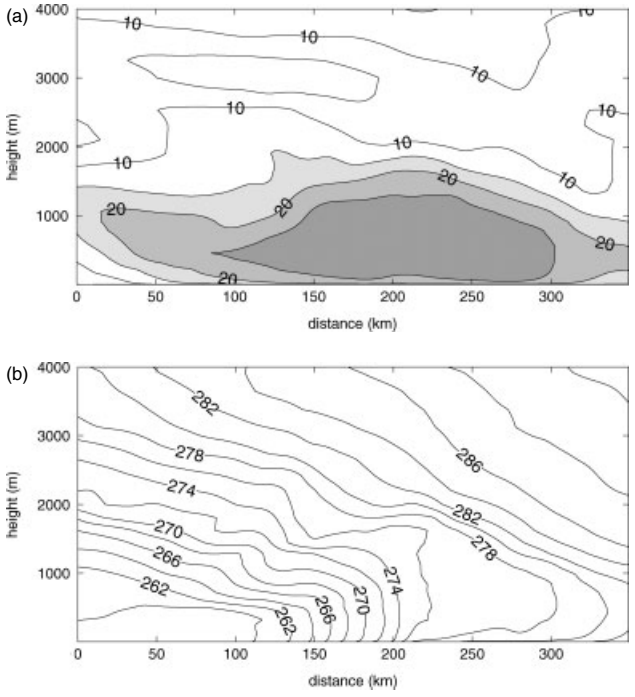

Figure 9. Simulated barrier flow at 1200 UTC on 2 March (T + 36 h) in the DSS cross-section, see Figure 6(c) for location. (a) Wind speed ($m\,s^{-1}$), contour interval 5 $m\,s^{-1}$ with wind speeds exceeding 15 $m\,s^{-1}$ shaded. (b) Equivalent potential temperature (K), contour interval 2 K.

with observations. Over the sea ice, there is a low-level inversion, although not as low or sharp as observed. The well-mixed boundary layer over the open water is capped by an inversion at about 2000 m.

Over the next 24 hours the winds strengthen as the pressure gradient tightens, from core wind speeds of 20 $m\,s^{-1}$ to 35 $m\,s^{-1}$ (Figure 7(c)). The maximum wind speed is found south of the Denmark Strait at 65°N where the cyclone centre is closest to the topography of Greenland and the pressure gradient is largest (Figures 6(c) and 7(c)). The eastern edge of the jet is sharp and coincides with the edge of the pressure gradient.

At lower levels, wind vectors and potential temperature give an indications of katabatic or drainage flow, e.g. in Scoresbysund (just south of Cape Tobin). This flow can to some extent be detected in Figure 7(b).

The dropsonde flight legs are located north of the maximum simulated wind speed (Figure 7(c)). The simulated flow in the DSS cross-section is shown in Figure 9. The simulated low-level jet is in quite good agreement with observations (Figure 4, right panels). It is confined below about 1800 m and has a broad core with wind speeds exceeding 28 $m\,s^{-1}$ capped by a layer of calm winds. However, the simulation does not capture the sharpness of the shear at the jet top. The equivalent potential temperature cross-section shows, as observed, a stable layer over the sea ice but a well-mixed ABL over open water. The temperatures over the sea ice are in quite good agreement with the observations, but over the open water the temperatures are too low. A tendency for MetUM simulations to have too cold surface layers over the ocean in this region was also found in a comparison of operational MetUM forecasts against GFDex low-level aircraft observations (Renfrew *et al.*, 2009). Above the well-mixed layer there is an increase in the equivalent potential temperature gradient but not the distinct temperature inversion seen in the observations. There is also a local maximum in the specific humidity above the jet, although again not as pronounced as in the observations (not shown).

The simulated flow in the DSN cross-sections also captures the main features of the flow well, but to a lesser extent the sharp shears (not shown). Note that in the northern part of the Denmark Strait the simulated wind speed close to Iceland (Figure 7) was too high. This is likely due to the orography of the northwestern peninsula not being well resolved.

In short, the simulation captures the synoptic and mesoscale flow quite well, with the exception of the sharp changes in e.g. wind speed and temperature at the top of the jet.

4.3. Simulated barrier flow: 5–6 March 2007

Figures 10-12 show the simulated mean sea level pressure, the barrier wind evolution and potential temperature at about 650 m height from 1200 UTC on 5 March to 1200 UTC on 6 March, every 12 hours. The mean sea level pressure field shows high pressure by Cape Tobin due to blocking. In the Denmark Strait and over the Irminger Sea, the pressure field changes as the cyclone moves in the region, from the isobars being almost parallel to the southeast coast of Greenland to, at 1200 UTC on 6 March, having moved away from the coast (Figure 10). The largest pressure gradient perpendicular

DOI: 10.1002/qj

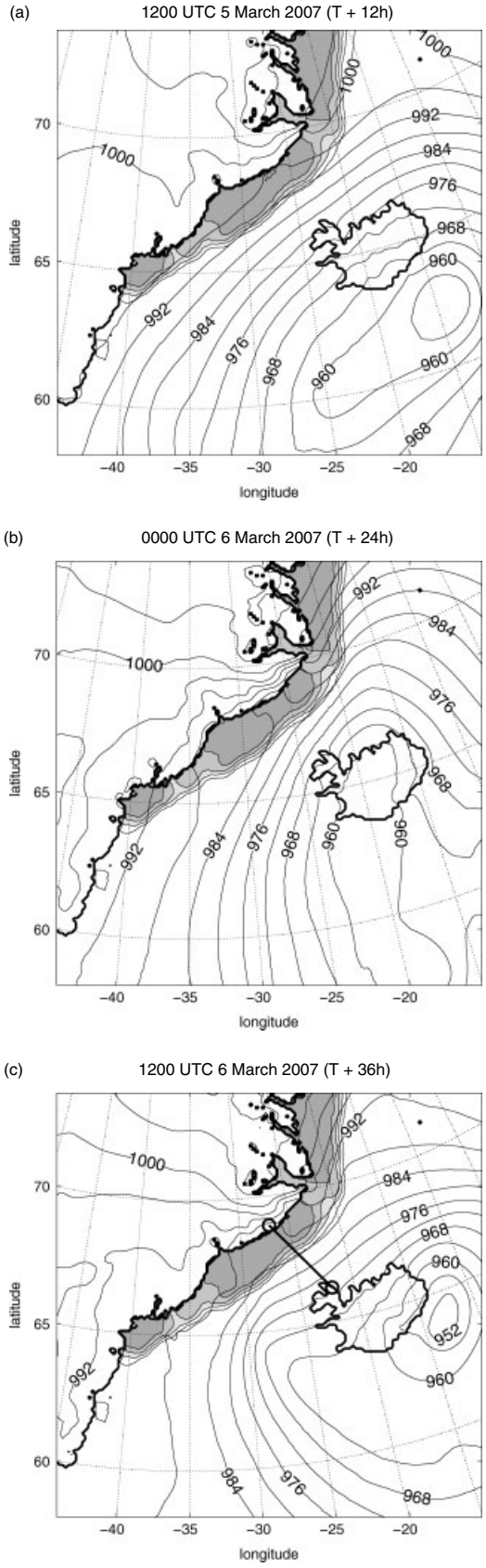

Figure 10. Simulated barrier flow for 5–6 March: mean sea level pressure (hPa). The simulation is initialized at 0000 UTC on 5 March. (a) 1200 UTC 5 March (T + 12 h), (b) 0000 UTC 6 March (T + 24 h) and (c) 1200 UTC 6 March (T + 36 h). The contour interval is 4 hPa. The shaded area represents the sea-ice concentration, shading interval 0.2. The bold line represents the location of the DSN cross-section.

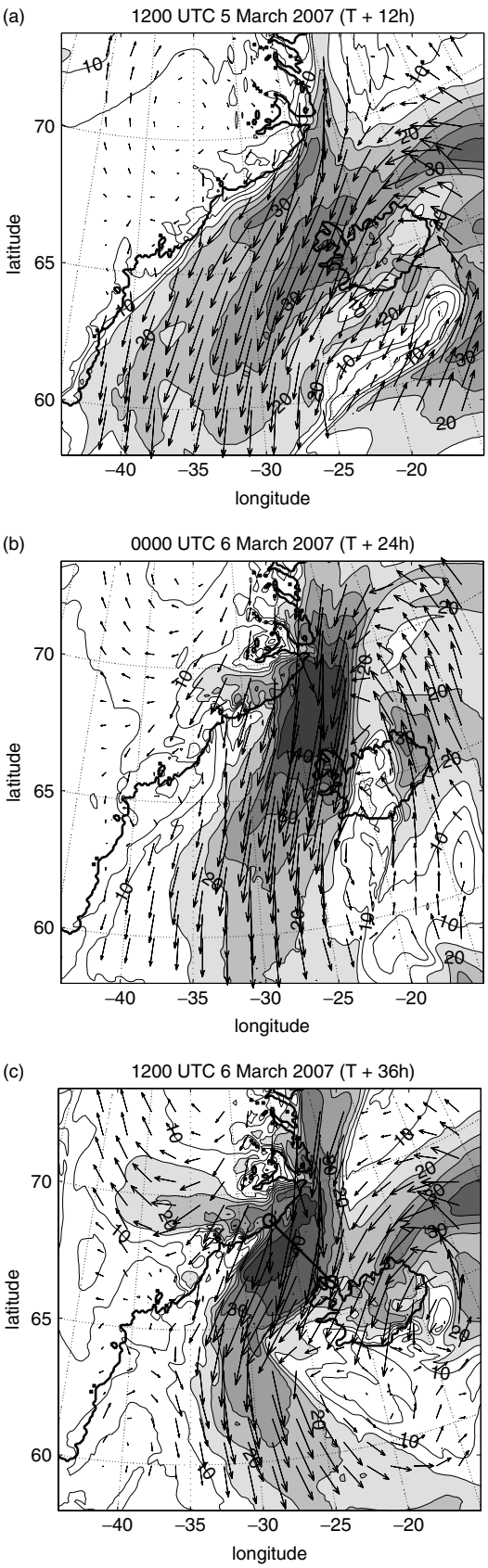

Figure 11. Simulated barrier flow for 5–6 March: wind speed ($m\,s^{-1}$, solid) and wind vectors at model level 12 ($\sim$ 650 m). The simulation is initialized at 0000 UTC on 5 March. (a) 1200 UTC 5 March (T + 12 h), (b) 0000 UTC 6 March (T + 24 h) and (c) 1200 UTC 6 March (T + 36 h). The contour interval is $5\,m\,s^{-1}$ and wind speeds exceeding $15\,m\,s^{-1}$ are shaded. The bold line represents the location of the DSN cross-section.

DOI: 10.1002/qj

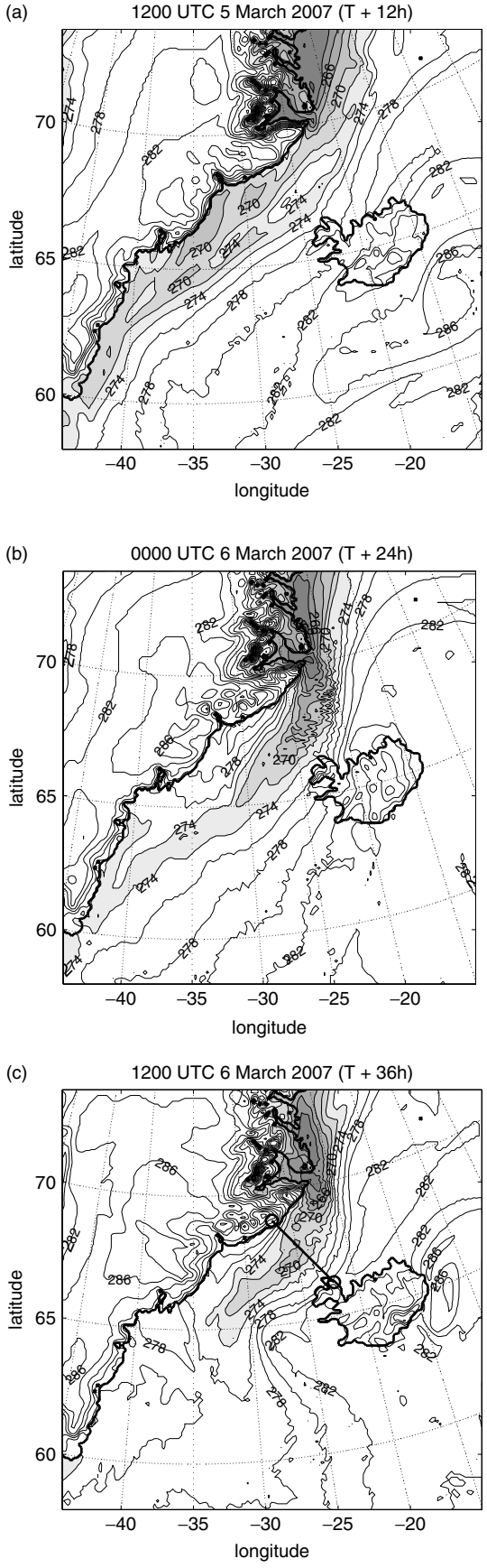

Figure 12. Simulated barrier flow for 5–6 March: potential temperature (K) at model level 12 (∼ 650 m). The simulation is initialized at 0000 UTC on 5 March. (a) 1200 UTC 5 March (T + 12 h), (b) 0000 UTC 6 March (T + 24 h) and (c) 1200 UTC 6 March (T + 36 h). The contour interval is 2 K and potential temperatures lower than 274 K are shaded. The bold line represents the location of the DSN cross-section.

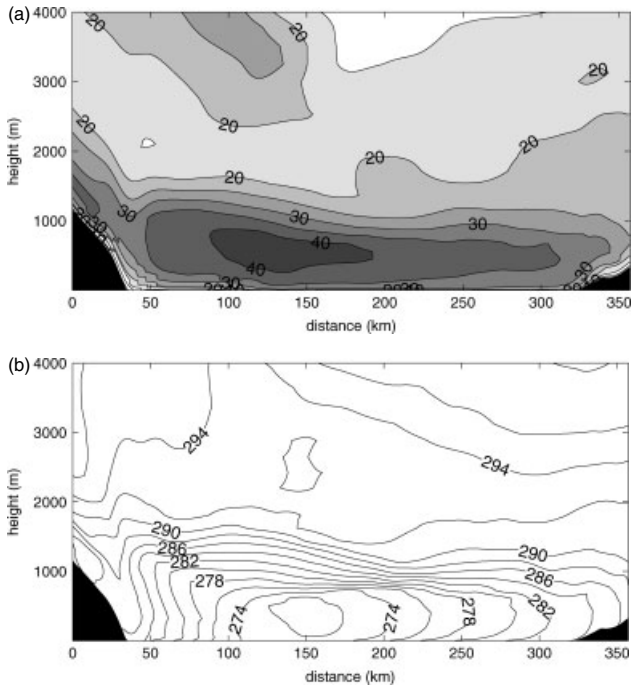

Figure 13. Simulated barrier flow at 1200 UTC on 6 March (T + 36 h) in the DSN cross-section, see Figure 10(a) for location. (a) Wind speed ($m\,s^{-1}$), contour interval $5\,m\,s^{-1}$ with wind speeds exceeding $15\,m\,s^{-1}$ shaded and (b) equivalent potential temperature (K), contour interval 2 K.

to the coast is just south of Cape Tobin, where the cyclone is closest to the orography. At 1200 UTC on 5 March the wind field shows *two* parallel low-level jets, a jet originating north of Cape Tobin hugging the coast closely and another broader jet slightly farther east associated with the synoptic cyclone located just south of Iceland (Figure 11(a)). The northerly-originating jet carries cold Arctic air along the coast of Greenland all the way to Cape Farewell (Figure 12(a)).

During the next 24 hours the barrier flow strengthens as the cyclone moves closer to Cape Tobin. The northern jet follows the east coast of Greenland until it reaches the cape. It then detaches from the coast (Figure 11(b)) and flows almost directly southward in the Denmark Strait and then cyclonically around the synoptic cyclone (Figure 11(c)). This results in a tongue of cold air emanating from Cape Tobin and flowing southward approximately in the middle of the Denmark Strait. The temperature difference at 0000 UTC on 2 March between the centre of the cold jet and the air by Greenland's coast is up to 10 K, over a distance of 150 km (Figure 12(b)). This large gradient was found in the observations 12 hours later when the jet in the Denmark Strait had a northerly wind direction, a very cold core and a temperature difference of 6–8 K at similar height, from the cold core towards Greenland (Figure 5, centre panels). At lower levels, flow can be detected out of Kangerdlussuaq fjord and in a few other locations along the southeastern coast (not shown).

The simulated flow in the DSN cross-section is shown in Figure 13. The simulated wind speed exceeds the observed one by about $5\,m\,s^{-1}$ (Figure 5, top right panel)

DOI: 10.1002/qj

but, as observed, it fills most of the Denmark Strait below a temperature inversion at roughly 1500 m. The vertical temperature gradient is large but not as sharp as the observed one. However, note that as observed, and in contrast with the flow on 2 March, there are high wind speeds above the temperature inversion, in general exceeding 15 m s^{-1}. These high wind speeds are due to frontal jets, as also evident in Figure 11. There is, as in the observations, a slight wind directional change at the temperature inversion with northerly flow below and northeasterly above. Associated with the overly strong jet are temperatures that are slightly too low, the jet core being about 2–3 K colder than observed.

As observed, the simulation shows that the low-level jet is dry, while above the temperature inversion the air is moist with a local maximum in specific humidity between the inversion and the mountain height. A cross-section along the dropsonde leg north of the Denmark Strait shows similar results (not shown).

In short, although the simulated flow pattern is in good agreement with the observations, the strength is overestimated. The jet wind speed is about 5 m s^{-1} higher than observed and the jet core is too cold. As in the simulation for 1–2 March, the temperature inversion capping the low-level jet is not as sharp as observed.

4.4. Model temperature initialization

Both simulations fail to simulate properly the extremely sharp temperature inversions capping the low-level jets. A comparison of the model initial temperature profile with a radiosonde ascent at Ittoqqoroormiit (Scoresbysund), close to Cape Tobin, at 0000 UTC on 5 March shows that the observed temperature inversion is poorly analysed in the initial conditions (Figure 14) and thus the analysed profile does not capture the observed boundary-layer structure. These well-defined inversions are rather common in winter, e.g. they were present at Ittoqqoroormiit during most of the GFDex field campaign, and it is likely that a failure in representing this cold boundary layer and the sharp top in the initial conditions leads to less pronounced temperature inversions and wind shear at the top of the simulated barrier winds.

5. Discussion

Although the barrier flows on 2 and 6 March had their maxima in different locations, they were forced by the same synoptic system. On 2 March the cyclone centre was over the Irminger Sea, resulting in the largest pressure gradient perpendicular to the coast (and the highest wind speed) at the southern edge of the Denmark Strait. On the other hand, on 6 March the cyclone centre was located by the southeast coast of Iceland, resulting in the largest pressure gradient perpendicular to the barrier (and the highest wind speed) in the northern part of the Denmark Strait. *In both cases the location of the cyclone centre relative to the orography of Greenland was a determining factor in the location of the peak values of the barrier flow.*

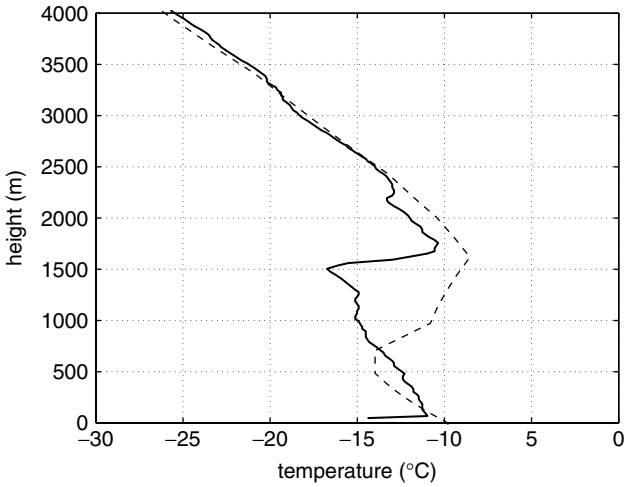

Figure 14. Temperature (°C) profiles at 0000 UTC on 5 March 2007 in Ittoqqoroormiit (Scoresbysund, 70°29′′N, 21°57′′E). The radiosonde ascent is shown with a solid, bold line and the MetUM analysis with a dashed line.

Furthermore, as has been illustrated, earlier the situation was ever-changing and therefore so was the barrier flow, both in magnitude and in location. The observations obtained during GFDex thus give snapshots of the ever-changing situation.

It is interesting to note that, as in Moore and Renfrew (2005), the low-level jet of 1–6 March was found in two regions at approximately 67°N and 65°N (Figures 7 and 11). In between these two regions the coastline is cut by a large fjord, Kangerdlussuaq, and here the high orography is farther inland than in the areas to the north and south (Figure 1). This means that synoptic cyclones moving into the region will first impinge upon the coast either to the south or north of the fjord, and that is where a low-level barrier jet develops, while the Kangerdlussuaq fjord itself is sheltered against the cyclones and thus the highest wind speeds.

The difference between Greenland barrier flow and classical barrier flow is emphasized by Figure 15, showing the geostrophic and ageostrophic components of the flow at 1200 UTC on 6 March. North of 70°N the jet is in approximately geostrophic balance and thus more of a classical barrier jet (Schwerdtfeger, 1975). However, in the Denmark Strait (67°–70°N) the ageostrophic component of the flow is comparable to the geostrophic component, and so the flow does not follow this classic force-balance model. Here the flow is *controlled by the synoptic cyclone and bounded by the orography*. South of the Denmark Strait, the flow turns cyclonically (away from the barrier) and becomes approximately geostrophic again. Furthermore, in contrast to the classical barrier flow, the Greenland barrier flow has a negligible wind component perpendicular to the barrier, resulting in the Rossby deformation radius ($L_R = Nh/f$), where f is the Coriolis parameter, which is commonly used to describe the width of classical barrier flows, being of little relevance to the flow here.

It has been shown that Greenland's orography modifies the flow over the Irminger Sea, resulting e.g. in

DOI: 10.1002/qj

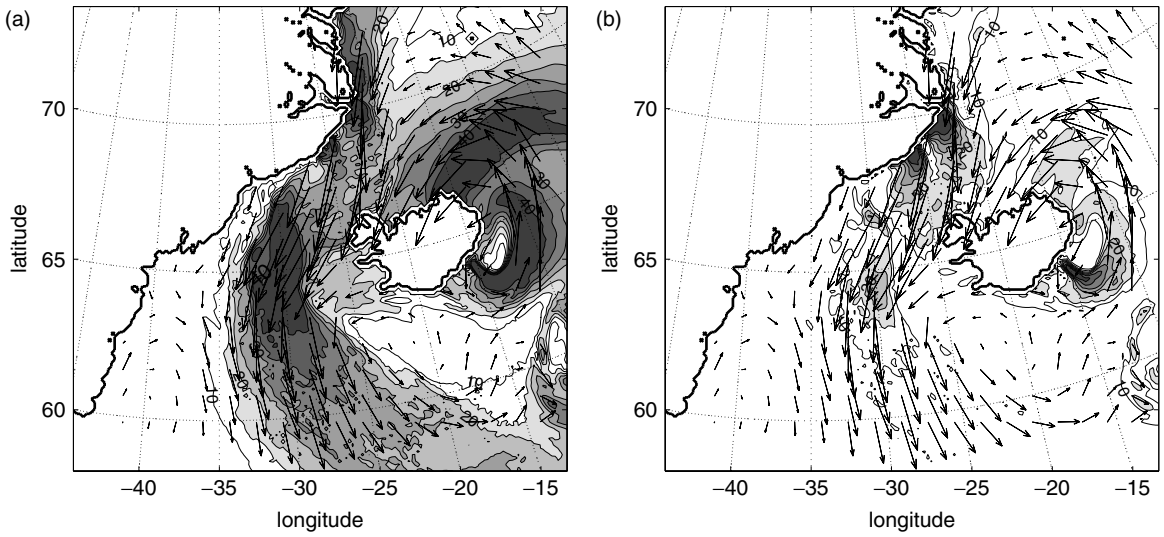

Figure 15. 1200 UTC on 6 March 2007 (T + 36 h): (a) geostrophic wind speed ($m\,s^{-1}$) and (b) ageostrophic wind speed ($m\,s^{-1}$) at model level 12 ($\sim$ 650 m) over the sea. The contour interval is $5\,m\,s^{-1}$, starting at $10\,m\,s^{-1}$, and wind speeds exceeding $15\,m\,s^{-1}$ are shaded. The vectors are total wind vectors.

quasi-stationary cyclones (Petersen *et al.*, 2003) and the development of baroclinic lee cyclones (Kristjánsson and McInnes, 1999). However, even in cases when the orography has little impact on the cyclone location it can have a large impact on the mesoscale by blocking the flow. Figure 16 shows mean sea level pressure and the wind field in the Greenland–Iceland region for a 36 hour simulation where the orography of Greenland has been removed (NoGreen). During reconfiguration, the model extrapolates the atmospheric initial conditions down to the surface. The MetUM is designed for different horizontal and vertical resolutions so this extrapolation is done without creating much noise. For the purposes of this experiment one can regard the synoptic situation over the ocean as 'comparable' to the one in the control simulations: the mean sea level cyclone centre is about a degree farther north in the NoGreen simulation than in the control simulation and the trough, found at 64°N in the control simulation, is found slightly farther north here, extending from the northwest peninsula of Iceland into the Denmark Strait.

In the absence of the orography, the snapshot at T + 36 h shows the flow northeast of the Denmark Strait to be diffluent, as there is a trough by the eastern coast of Greenland, moving westward. In the control simulation the flow pattern is of a more stationary character, with confluent flow in this region caused by flow blocking by the orography. There are still relatively high wind speeds in the Denmark Strait in the NoGreen simulation, exceeding $25\,m\,s^{-1}$. However, these high wind speeds are frontal jets related to the cyclone itself, rather than barrier winds. Such frontal jets are also a feature of the control simulation, e.g. curving to the northeast around Iceland in Figure 11(a). In the control simulation these jets ascend over the northerly barrier jet (Figures 5 and 13); however, in the NoGreen simulation they stay close to the surface (not shown). Although the wind speed in the Denmark Strait is relatively high, it does not compare with the wind speeds in the control simulation of up to about $42\,m\,s^{-1}$. In short, *the NoGreen versus control comparison illustrates the* $\sim 20\,m\,s^{-1}$ *enhancement of the barrier flow's peak winds through blocking.*

A similar experiment initialized at 0000 UTC on 1 March had the synoptic cyclone not moving northward over the Irminger Sea in the NoGreen simulation. This results in a different synoptic situation over the ocean than in the control simulation.

Two simulations with Iceland removed were also performed, but the results differed little from the control simulations. Iceland's orography can result in flow distortion and high winds around Iceland (Haraldur Ólafsson, personal communication), but our experiments suggest that the impact on Greenland barrier flows is small.

The air in these Greenland barrier jets is not directly associated with the synoptic cyclones; rather at low levels it has an Arctic origin north of Cape Tobin, with a contribution from the ice sheet through katabatic or drainage flow. This cold and dry air is drawn southward by the synoptic activity in the Greenland–Iceland region. It can be seen clearly in the observations (Figures 3–5) that the low-level jet is colder, drier and has a more northerly wind direction than the air above. The simulations agree with the observations but also emphasize the non-stationarity of the barrier flow (Figures 6–13).

The different origin of the air in the jet from the air above can also be seen in backward trajectories. Figure 17 shows 48 hour backward trajectories from ECMWF operational analysis. The trajectories were initialized in the southern Denmark Strait at 1200 UTC on 2 March and 6 March at 900 hPa, the approximate level of maximum wind speed, and at 800 hPa, above the low-level jet. The trajectory time step was 30 min and the spatial and temporal resolution of the analysis is 1.125° and 6 h, respectively.

The panels show clearly that the low-level air in the Denmark Strait had a northern origin, while the air above

DOI: 10.1002/qj

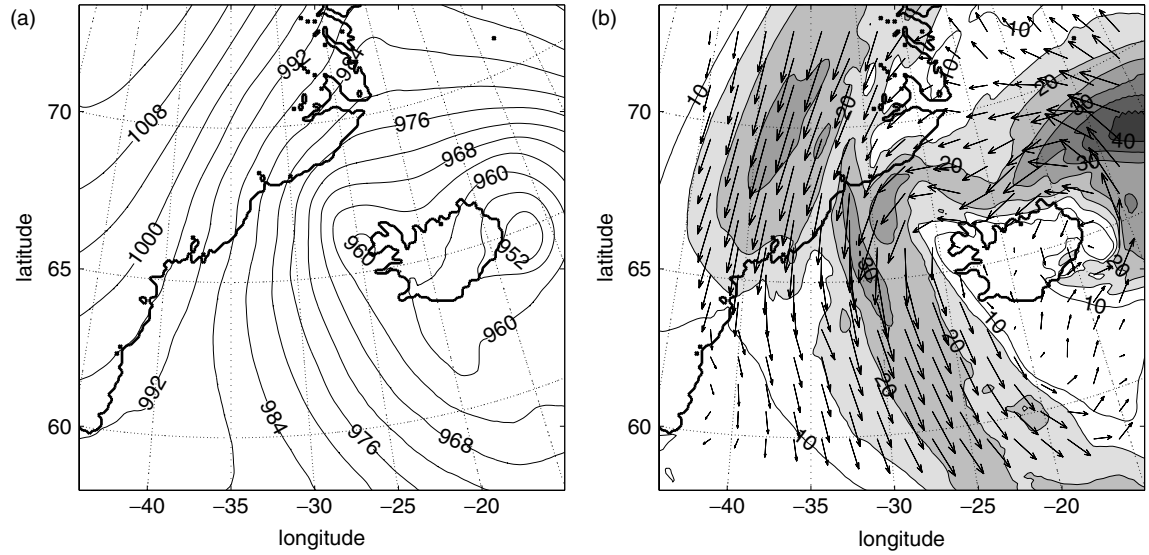

Figure 16. NoGreen, 1200 UTC on 6 March (T + 36 h): (a) mean sea level pressure (hPa) and (b) wind speed ($m\,s^{-1}$) and wind vectors at model level 12 ($\sim$ 650 m) in the absence of Greenland's orography. Wind speeds exceeding $15\,m\,s^{-1}$ are shaded.

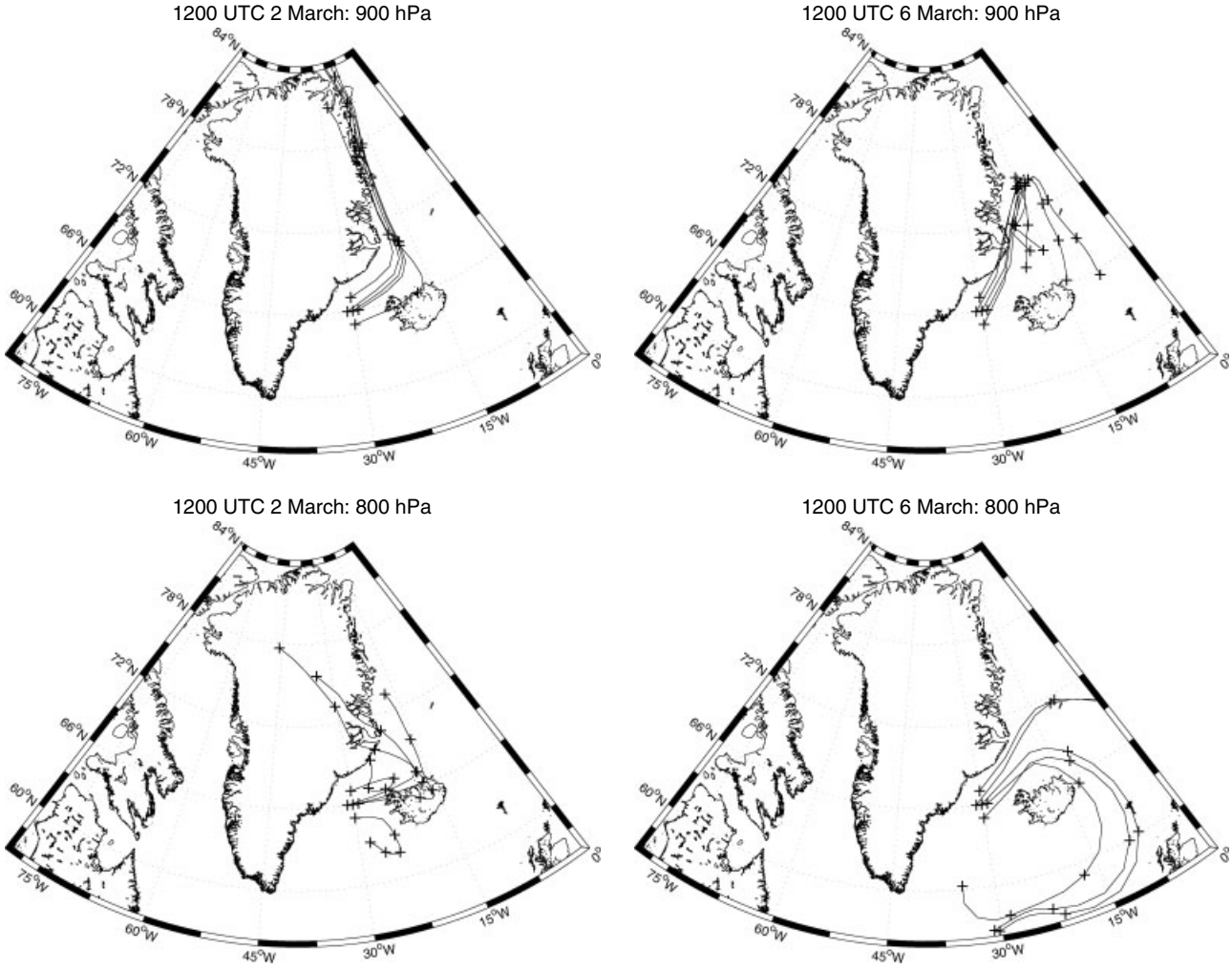

Figure 17. ECMWF 48 hour backwards trajectories with the location every 12 hours marked with a cross. Left panels: initialized on 2 March. Right panels: initialized on 6 March. Top panels initialized pressure 900 hPa. Bottom panels: initialized pressure 800 hPa.

DOI: 10.1002/qj

had a more southerly origin, related to the synoptic situation in the region. Most of the 800 hPa backward trajectories show that the air originated at lower levels and was lifted over the low-level jet in the Denmark Strait (not shown). This is supported by the observations of a strong temperature inversion capping the low-level jet and moist air above the inversion (Figure 4).

There are indications in the simulations of katabatic or drainage flow contributing to the barrier jet. The synoptic forcing is important to enforce katabatic winds in East Greenland, e.g. synoptic cyclones can increase the horizontal temperature difference in the region by warm air advection as well as enforcing drainage flow from the ice sheet through an increased pressure gradient normal to the coast (Klein and Heinemann, 2002). Although our simulations show that these Greenland barrier jets are primarily synoptically forced, katabatic or drainage flow may play a more prominent role in other cases.

Some similarities can be found between the Greenland barrier flow and the hybrid barrier jets by the west coast of the USA (Neiman *et al.*, 2006; Olson *et al.*, 2007), i.e. offshore maximum wind speed and cold jet core, but there are also fundamental differences. The hybrid jets are primarily fed by gap flow. In contrast, although there is a contribution from katabatic or drainage flow to the Greenland barrier flow, the jet is mainly fed by cold, dry air drawn southward by the synoptic forcing and bounded by the steep orography. The jet is also capped far below mountain height by a strong temperature inversion, separating the cold jet from the relatively warm and moist cyclone air. It is common for cyclones to become quasi-stationary in the Greenland–Iceland region, thus maintaining large pressure gradients normal to the steep Greenland coast. This can result in barrier flow in the Denmark Strait for a few days, with the location depending on the cyclone location. This is again quite different from the hybrid jets, which are typically pre-frontal phenomena caused by landfalling cyclones. Due to the complexity of the Greenland barrier flow, it is clear that the criteria for simple scaling are not met.

Along the sea-ice edge, changes in surface drag and heat flux can drive local jets (Drüe and Heinemann, 2001; Orr *et al.*, 2005). It is likely that such jets were present during the barrier flow described here, especially on 1–2 March, but due to the small scale of these jets we were unable to detect them in the dropsonde observations and numerical simulations. Sensitivity studies with different sea-ice cover in the Denmark Strait did not change the broad evolution of the barrier winds, suggesting that surface forcing was not of primary importance for these cases. Further studies using the flight-level data and higher resolution simulations are planned, and these may be able to shed light on the importance of sea-ice-edge jets for the barrier flow.

The fact that the barrier jets are strong, cold and dry results in enhanced air–sea heat fluxes. A low-level flight leg was flown in the Denmark Strait on 2 March, and the bulk sensible and latent heat fluxes obtained were as high as 350 and 230 $W\,m^{-2}$, respectively, under the Denmark Strait North flight leg. The MetUM fluxes in the Denmark Strait are in good agreement with these observations, $\sim$300 and $\sim$250 $W\,m^{-2}$, respectively, with both exceeding 500 $W\,m^{-2}$ just south of the Denmark Strait. On 6 March no heat flux observations were obtained within the barrier jet in the Denmark Strait, although some flux measurements were obtained just west of Iceland (Petersen and Renfrew, 2009). The MetUM sensible and latent heat fluxes on 6 March are both 300–400 $W\,m^{-2}$ (not shown). On 6 March the barrier results in a doubling of the wind speeds and thus a doubling of the heat fluxes, compared with the case of no barrier. Thus, the observations and model simulations are in good agreement with the current view that the strong barrier winds in this region can have significant impact on the ocean. Further studies of the air–sea interaction associated with these barrier flows is also planned.

6. Conclusions

During the GFDex, unique *in situ* observations of barrier flow in the Denmark Strait were obtained in four missions. In this article we present observations from 1, 2 and 6 March 2007 when dropsondes were launched in the Denmark Strait and north of the Denmark Strait.

This is the first time that vertical profiles of the Greenland barrier flow have been obtained, and the observations give valuable insight into the characteristics of the barrier flow.

- There was a large temporal variation in the barrier flow, suggesting a strong synoptic control of this mesoscale feature.
- Over the open ocean the boundary layer was well-mixed, approximately neutrally stratified, while over the sea ice there was a stable boundary layer. There were indications of lower wind speeds just above the sea ice compared with those over the open water, due to a larger surface roughness in the presence of sea ice.
- The observed barrier jet was confined below about 1500–2000 m, well below mountain height.
- The observations indicate two air masses below mountain height: a cold and dry barrier-jet air mass of northern origin and a warmer and more moist air mass advected into the region by the synoptic system. There was a sharp temperature inversion at the boundary between the air masses and a wind directional change between the barrier jet and the flow above.

To shed more light on the situation and the evolution, numerical simulations of the flow in the Greenland–Iceland region were performed with the UK Met Office Unified Model in a limited-area mode. The numerical simulations were in reasonably good agreement with the observations. They showed that the barrier jet originated north of Cape Tobin and the flow was drawn southward by the synoptic cyclone. Furthermore, the simulations emphasized that the location of the maximum barrier flow is highly dependent on the location of the cyclone centre

DOI: 10.1002/qj

relative to the orography of Greenland, as suggested by Moore and Renfrew (2005). Numerical simulations without Greenland showed that the orographic blocking of Greenland results in a doubling of the low-level winds in the Denmark Strait and thus roughly a doubling of the surface heat fluxes.

ECMWF analysis backward trajectories from the Denmark Strait are in agreement with both simulations and observations in showing that the air in the lowest levels had Arctic origin, while the air above the temperature inversion was advected into the region at low levels by the synoptic cyclone and ascended over the jet.

Our analysis has shown that these Greenland barrier flows are not simply classic barrier flows, as described by e.g. Schwerdtfeger (1975) or Parish (1982, 1983), nor are they primarily hybrid barrier flows, i.e. those with a significant forcing from gap or drainage flows as described by e.g. Loescher *et al.* (2006) or Olson *et al.* (2007). Instead these Greenland barrier flows have a significant ageostrophic component, related to the close proximity of the synoptic cyclone, so in this sense they are more related to the Appalachian or Rocky Mountain cold-air damming events described by Bell and Bosart (1988) and Colle and Mass (1995) respectively, as the air mass in the northerly barrier jet originates north of Cape Tobin but is controlled by the synoptic-scale systems. Based on these cases, barrier flows in the Greenland–Iceland region are therefore mesoscale features controlled by the synoptic-scale flow.

Acknowledgements

The authors acknowledge the efforts of everyone involved in planning and carrying out GFDex. The support of FAAM, DirectFlight and Avalon during the field campaign was greatly appreciated. The ECMWF backward trajectories were calculated using the British Atmospheric Data Centre's (BADC) Trajectory Service. Discussions with Haraldur Ólafsson were greatly appreciated. This study was funded by the Natural Environmental Research Council (NERC) (NE/C003365/1).

References

Andreas EL, Persson POG, Jordan RE, Horst TW, Guest PS, Grachev AA, Fairall CW. 2005. Parameterizing the turbulent surface fluxes over summer sea ice. *8th Conference on Polar Meteorology and Oceanography*. Am. Meteorol. Soc.: San Diego, CA. p. J1.15.

Bell GD, Bosart LF. 1988. Appalachian cold-air damming. *Mon. Weather Rev.* **116**: 137–161.

Brunke MA, Zhou M, Zeng X, Andreas EL. 2006. An intercomparison of bulk aerodynamic algorithms used over sea ice with data from the Surface Heat Budget for the Arctic Ocean (SHEBA) experiment. *J. Geophys. Res.* **111**: C09001. doi:10.1029/2005JC002907.

Chen WD, Smith RB. 1987. Blocking and deflection of airflow by the Alps. *Mon. Weather Rev.* **115**: 2578–2597.

Colle BA, Mass CF. 1995. The structure and evolution of cold surges east of the Rocky Mountains. *Mon. Weather Rev.* **123**: 2577–2610.

Davies T, Cullen MJP, Malcolm AJ, Mawson MH, Staniforth A, White AA, Wood N. 2005. A new dynamical core for the Met Office's global and regional modelling of the atmosphere. *Q. J. R. Meteorol. Soc.* **131**: 1759–1782.

Doyle JD, Shapiro MA. 1999. Flow response to large-scale topography: the Greenland tip jet. *Tellus* **51A**: 728–748.

Drüe C, Heinemann G. 2001. Airborne investigation of Arctic boundary-layer fronts over the marginal ice zone of the Davis Strait. *Boundary-Layer Meteorol.* **101**: 261–292.

Durran DR. 1990. Mountain waves and downslope winds. *Atmospheric Prosesses over Complex Terrain, Meteor. Monogr. 45*. Blumen W. (ed.). Am. Meteorol. Soc.: Boston. pp. 59–81.

Edwards JM. 2007. Oceanic latent heat fluxes: Consistency with the atmospheric hydrological and energy cycles and general circulation modeling. *J. Geophys. Res.* **112**: D06115. doi:10.1029/2006JD007324.

Essery R, Best M, Cox P. 2001. *MOSES 2.2 technical documentation*. Hadley Centre Technical Note 30. Met Office: Exeter, UK. http://www.metoffice.gov.UK/publications/HCTN/HCTN_30.pdf.

Haine T, Zhang S, Moore GWK, Renfrew IA. 2009. On the impact of high-resolution, high-frequency meteorological forcing on Denmark Strait ocean circulation. *Q. J. R. Meteorol. Soc.* **135**: 2067–2085.

Heinemann G. 1999. The KABEG'97 field experiment: An aircraft-based study of katabatic wind dynamics over the Greenland ice sheet. *Boundary-Layer Meteorol.* **93**: 75–116.

Klein T, Heinemann G. 2002. Interaction of katabatic winds and mesocyclones near the eastern coast of Greenland. *Meteorol. Appl.* **9**: 407–422.

Kristjánsson JE, McInnes H. 1999. The impact of Greenland on cyclone evolution in the North Atlantic. *Q. J. R. Meteorol. Soc.* **125**: 2819–2834.

Lock AP, Brown AR, Bush MR, Martin GM, Smith RNB. 2000. A new boundary layer mixing scheme. Part I: Scheme description and single-column model tests. *Mon. Weather Rev.* **128**: 3187–3199.

Loescher KA, Young GS, Colle BA, Windstead NS. 2006. Climatology of barrier jets along the Alaskan coast. Part I: Spatial and temporal distribution. *Mon. Weather Rev.* **134**: 437–453.

Lüpkes C, Birnbaum G. 2005. Surface drag in the Arctic marginal sea-ice-zone: A comparison of different parameterisation concepts. *Boundary-Layer Meteorol.* **117**: 179–211. doi:10.1007/s10546-005-1445-8.

Martin C. 2007. *ASPEN (Atmospheric sounding processing environment) user manual*. Technical report. National Center for Atmospheric Research: Boulder, CO.

Martin GM, Bush MR, Brown AR, Lock AP, Smith RNB. 2000. A new boundary layer mixing scheme. Part II: Tests in climate and mesoscale models. *Mon. Weather Rev.* **128**: 3200–3216.

McInnes H, Kristjánsson JE, Schyberg H. 2009. An assessment of a Greenland lee cyclone during the Greenland Flow Distortion Experiment: An observational approach. *Q. J. R. Meteorol. Soc.* **135**: 1968–1985.

Moore GWK. 2003. Gale force winds over the Irminger Sea to the east of Cape Farewell, Greenland. *Geophys. Res. Lett.* **17**: 1894. doi:1029/2003GL018 012.

Moore GWK, Renfrew IA. 2005. Tip jets and barrier winds: a QuikSCAT climatology of high wind speed events around Greenland. *J. Climate* **18**: 3713–3725.

Neiman PJ, Ralph FM, White AB, Parrish DD, Holloway JS, Bartels DL. 2006. A multiwinter analysis of channeled flow through a prominent gap along the northern California coast during CALJET and PACJET. *Mon. Weather Rev.* **134**: 1815–1841.

Olson JB, Colle BA, Bond NA, Winstead N. 2007. A comparison of two coastal barrier jet events along the Southeast Alaskan coast during the SARJET field experiment. *Mon. Weather Rev.* **135**: 3642–3663. doi:10.1175/MWR3448.E1.

Orr A, Hunt J, Capon R, Sommeria J, Cresswell D, Owinoh A. 2005. Coriolis effect on wind jets and cloudiness along coasts. *Weather* **60**: 291–299. doi:10.1256/wea.219.04.

Outten S, Renfrew IA, Petersen GN. 2009. An easterly tip jet off Cape Farewell, Greenland. Part II: Simulations and dynamics. *Q. J. R. Meteorol. Soc.* **135**: 1934–1949 .

Pagowski M, Moore GWK. 2001. A numerical study of an extreme cold-air outbreak over the Labrador Sea: Sea ice, air–sea interaction, and development of polar lows. *Mon. Weather Rev.* **129**: 47–72.

Parish TR. 1982. Barrier winds along the Sierra Nevada Mountains. *J. Appl. Meteorol.* **21**: 925–930.

Parish TR. 1983. The influence of the Antarctic Peninsula on the wind field over the western Weddell Sea. *J. Geophys. Res.* **88**: 2684–2692.

Petersen GN, Renfrew IA. 2009. Aircraft-based observations of air-sea fluxes over Denmark Strait and the Irminger Sea during high wind speed conditions. *Q. J. R. Meteorol. Soc.* **135**: 2030–2045.

Petersen GN, Ólafsson H, Kristjánsson JE. 2003. Flow in the lee of idealized mountains and Greenland. *J. Atmos. Sci.* **60**: 2183–2195.

Pickart RS, Spall MA, Ribergaard MH, Moore GWK, Milliff RF. 2003a. Deep convection in the Irminger Sea forced by the Greenland tip jet. *Nature* **424**: 152–156.

Pickart RS, Straneo F, Moore GWK. 2003b. Is the Labrador Sea Water formed in the Irminger basin? *Deep-Sea Res. I* **50**: 23–52.

Renfrew IA, Moore GWK. 1999. An extreme cold-air outbreak over the Labrador Sea: Roll vortices and air–sea interaction. *Mon. Weather Rev.* **127**: 2379–2394.

Renfrew IA, Moore GWK, Kristjánsson JE, Ólafsson H, Gray SL, Petersen GN, Bovis K, Brown PRA, Føre I, Haine T, Hay C, Irvine EA, Lawrence A, Ohigashi T, Outten S, Pickart RS, Shapiro M, Sproson D, Swinbank R, Woolley A, Zhang S. 2008. The Greenland Flow Distortion experiment. *Bull. Am. Meteorol. Soc.* **89**: 1307–1324.

Renfrew IA, Petersen GN, Sproson D, Moore GWK, Adiwidjaja H, Zhang S, North R. 2009. A comparison of aircraft-based surface-layer observations over Denmark Strait and the Irminger Sea with meteorological analyses and QuikSCAT winds. *Q. J. R. Meteorol. Soc.* **135**: 2046–2066.

Revell MJ, Copeland JH, Larsen HR, Wratt DS. 2002. Barrier jets around the Southern Alps of New Zealand and their potential to enhance alpine rainfall. *Atmos. Res.* **61**: 277–298.

Sampe T, Xie SP. 2007. Mapping high sea winds from space. *Bull. Am. Meteorol. Soc.* **88**: 1965–1978.

Schwerdtfeger W. 1975. Effect of Antarctic Peninsula on the temperature regime of the Weddel Sea. *Mon. Weather Rev.* **103**: 45–51.

Scorer RS. 1988. Sunny Greenland. *Q. J. R. Meteorol. Soc.* **114**: 3–29.

Skeie RB, Kristjánsson JE, Ólafsson H, Røsting B. 2006. Dynamical processes related to cyclone development near Greenland. *Meteorol. Z.* **15**: 147–156.

Stark JD, Donlon CJ, Martin MJ, McCulloch ME. 2007. 'OSTIA: An operational, high resolution, real time, global sea surface temperature analysis system.' In *OCEANS '07 IEEE Aberdeen, Conference Proceedings. Marine challenges: Coastline to deep sea*. IEEE: Piscataway, NJ.

van den Broeke MR, Gallée H. 1996. Observations and simulations of barrier winds at the western margin of the Greenland ice sheet. *Q. J. R. Meteorol. Soc.* **122**: 1365–1383.

von Hann JF. 1866. Zur Frage über den Ursprung des Föhns. *Zeit. Osterreich Ges. Met.* **1**: 257–263.

Webster S, Brown AR, Cameorn DR, Jones CP. 2003. Improvements to the representation of orography in the Met Office Unified Model. *Q. J. R. Meteorol. Soc.* **129**: 1989–2010. doi:10.1256/qj.02.133.